Design of Machines and Structures, Vol. 16, No. 1 (2026), pp. 18–40.
https://doi.org/10.32972/dms.2026.002

NUMERICAL INVESTIGATION OF VORTEX GENERATOR POSITION EFFECTS ON THERMAL-HYDRAULIC PERFORMANCE IN A CORRUGATED CHANNEL

AIMEN TANOUGAST – KRISZTIÁN HRICZÓ

University of Miskolc, Institute of Mathematics
H-3515, Miskolc- Egyetemváros
[1]tanougast.aimen@uni-miskolc.hu, [2]krisztian.hriczo@uni-miskolc.hu
[1]https://orcid.org/0009-0004-1928-3482, [2]https://orcid.org/0000-0003-3298-6495

Abstract: Improving heat transfer in compact heat exchangers is essential for achieving better thermal efficiency, particularly in corrugated channels where the geometry strongly influences the flow structure. This study numerically examines the thermal and hydraulic performance of a corrugated channel fitted with vortex generators (VGs), focusing on VG streamwise position effects. Three positions (d = –2, 0, and +2) were analysed using ANSYS Fluent with the SST k–ω turbulence model. Results indicate that placing VGs near the corrugation entrance (d = –2) provides the highest heat transfer enhancement (≈121%) and the maximum Performance Evaluation Criterion (PEC) of 0.96, although accompanied by a higher pressure drop (approximately 12.5 times higher than the baseline case). Optimizing VG placement improves overall heat exchanger performance.

Keywords: *Corrugated channel; Vortex generator; Heat transfer enhancement; CFD simulation; SST k–ω model*

1. INTRODUCTION

Improving heat transfer using passive enhancement techniques is essential for increasing the thermal efficiency of many engineering systems. This method mainly depends on altering the flow channel geometry or adding enhancement devices such as vortex generators (VGs) or nanofluids to strengthen the heat exchange process. Generally, passive techniques operate without the need for external power or extra energy input, which makes them easier to implement, more economical, and suitable for practical applications (Shah, Pan, Ibrahim, Saeed, & Ibrahim, 2022), (Samadifar & Toghraie, 2018), (Tanougast, Omle, & Hriczó, 2025), (Omle, Askar, & Kovács, 2024).

Nomenclature

SYMBOLS

VGs	Vortex generators
WVGs	Without vortex generators
PE	The percentage enhancement
PR	The pressure drop ratio
PEC	The performance evaluation criterion
k	Turbulent kinetic energy [m^2/s^2]
K	Thermal conductivity [W/(m K)]
f	Friction factor
q_w	Heat flux [W/m^2]
Re	Reynolds number
Nu	Nusselt number
h	Heat transfer coefficient [$W/(m^2$ K)]
P	Pressure [Pa]
T	Temperature [K]
u, v	Velocity components [m/s]
x, y	Cartesian coordinates [mm]
G	The production term in various transport equations
Cp	Specific heat [J/(kg K)]

GREEK LETTERS

ω	Specific dissipation rate [s^{-1}]
μ	Dynamic viscosity [N m/s^2]
μ_t	Turbulent dynamic viscosity [N m/s^2]
σ_k, σ_ω	Empirical constant for turbulence model
μ	Dynamic viscosity [N m/s^2]
ρ	Density [kg/m^3]
ΔP	Pressure drop [Pa]
τ	Shear stress [Pa]
ρ	Density [kg/m^3]

SUBSCRIPTS

w	Wall
av	Average
i, j	Cartesian coordinates indices

Heat transfer enhancement is often achieved using corrugated channel geometries, as they can provide a significant improvement in thermal performance. Several experimental and numerical studies have analysed their behaviour, and the results consistently show that these channels are effective in increasing heat transfer efficiency (Pehlivan, Taymaz, & İslamoğlu, 2013), (Ajeel, Salim, & Hasnan, 2019), (Wang & Chen, 2002), (Omle, Kovács, & Bolló, 2023), (Omle, Askar, & Kovács, 2024). (Ajeel R. , et al., 2019) examined a half-sinusoidal corrugated design combined with nanoparticles through numerical and experimental analysis. When comparing corrugated and straight channels, they found that the corrugated geometry offered higher thermal performance, making it a more suitable design for heat transfer enhancement. Corrugated channels have shown promising results in improving heat transfer, although they also come with a pressure drop penalty (Elshafei, Awad, El-Negiry, & Ali, 2010), (Naphon, 2007). The corrugated shape generates recirculation regions in the flow, which enhance mixing and improve heat transfer. This enhancement can be increased further by adding VGs, as they intensify fluid mixing and lead to better overall thermal performance.

VGs are among the most effective techniques for enhancing the heat transfer. They help control and manipulate the fluid flow by directing it toward specific regions, increasing the contact between the fluid and the surface and improving the thermal efficiency (Promvonge, Promthaisong, & Skullong, 2022), (Asaadi & Abdi, 2021), (Shlash & Koç, 2022), (Ismail, Ali, & Pereira, 2025). When applied to corrugated channels, VGs can reduce or eliminate the recirculation zones created by the corrugated geometry, leading to better flow distribution and higher overall thermal

performance (Wu, Liu, Yu, Liu, & Liu, 2022), (Tanougast & Hriczó, 2025), (Kotšmíd & Brodnianská, 2022). (Modi & Rathod, 2019) examined three VG configurations –sinusoidal, wavy, and elliptical curved rectangular winglets– installed in a semi-circular corrugated channel. Their findings showed that the curved and wavy designs produced greater heat transfer enhancement because they guided the flow more smoothly toward the channel walls, increasing fluid-surface interaction and improving overall thermal performance. (Brodnianská & Kotšmíd, 2023) investigated cylindrical VGs in a novel wavy corrugated channel and found that they significantly enhanced heat transfer and thermal performance, although with a slight increase in pressure drop, achieving a maximum thermal performance factor of approximately 0.82. (Tanougast & Hriczó, 2025) examined the effect of two-pair winglet VGs on a semi-circular corrugated channel. The VGs enhanced heat transfer by reducing the recirculation zones and thinning the thermal boundary layer, achieving a Performance Evaluation Criterion (PEC) of 0.88. In a related study, (Tanougast, Bessaih, & Hriczó, 2025) investigated a single-body VG with three shapes (concave up, concave down, and straight) in the same channel. They found that the single-body VG configuration achieved the highest overall performance in terms of PEC = 0.94. However, the concave-up configuration produced the highest heat transfer enhancement, with a slightly lower PEC = 0.93.

VGs work effectively in combination with corrugated channels, particularly semi-circular designs, where they enhance heat transfer performance. Although many studies have examined different VG configurations and two-pair arrangements, there is still a lack of research on the optimal placement of a single-body VG. The position of the VG plays an important role in determining both thermal and hydraulic behaviour. This work builds on the study of (Tanougast, Bessaih, & Hriczó, 2025), who used single-body VGs due to their good compatibility with corrugated geometries and superior performance compared to two-pair designs. The analysis is carried out in a 2D domain, focusing on the main flow direction and recirculation zones to better understand heat transfer mechanisms. Such configurations are particularly relevant for heat exchanger applications, where proper VG placement can improve thermal efficiency while keeping pressure losses under control.

2. MODEL DESCRIPTION

2.1. Numerical model

The semi-circular corrugated channel considered in this study consists of an inlet section (L1 = 200 mm), a test section (L2 = 200 mm), and an outlet section (L3 = 100 mm). The inlet and outlet were extended beyond the channel height (H)

to ensure fully developed flow and avoid backflow (Their, Hamad abed, Azeez, & Mohsin, 2023). The channel has a maximum height of 10 mm and a minimum height of 5 mm, with a wavelength (P) of 10 mm and a pitch diameter (D) of 5 mm. Concave-up vortex generators (CUVGs) were installed in the channel, and three streamwise positions relative to the corrugation entrance were considered: d = −2 mm, 0 mm, and +2 mm. Water was used as the working fluid in all simulations.

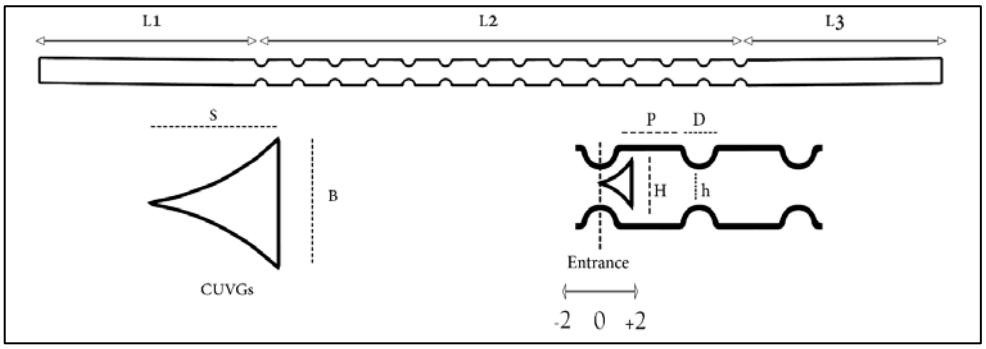

Figure 1. *Numerical model of the corrugated channel with vortex generators (VGs)*

2.2. Governing equations

In this work, water is considered a viscous, Newtonian, and incompressible fluid with constant thermophysical properties and the flow is assumed to be steady and turbulent (Tanougast & Hriczó, 2025). A two-dimensional simulation in the x-y plane is used to simplify the analysis while capturing the main flow features. This allows detailed observation of the streamwise flow, recirculation regions, and thermal boundary layer development, in line with previous 2D studies (Modi & Rathod, 2019), (Their, Hamad abed, Azeez, & Mohsin, 2023), (Akcay, 2022). Body forces are neglected due to their negligible effect on the flow behaviour. The governing equations for mass, momentum, and energy conservation in Cartesian coordinates are formulated as follows (Neves, Soares, & Rouboa, 2022):
Continuity equation

$$\frac{\partial \overline{u_i}}{\partial x_i} = 0, \tag{1}$$

where $\overline{u_i}$ is the mean velocity vector.

Momentum equation

$$\bar{u}_j \frac{\partial(\bar{u}_i)}{\partial \mathrm{x_j}} = -\frac{1}{\rho}\frac{\partial \bar{P}}{\partial x_i} + \frac{\partial}{\partial x_j}\left(v\frac{\partial \bar{u}_i}{\partial x_j} - \overline{u'_i u'_j}\right), \quad (2)$$

where $\bar{P}$ is the mean static pressure, ρ is the fluid density, and v is the kinematic viscosity.

Energy equation

$$\rho C_p \bar{u}_j \frac{\partial(\bar{T})}{\partial x_j} = \frac{\partial}{\partial x_j}\left(K\frac{\partial \bar{T}}{\partial x_j} - \rho Cp\overline{u'_j T'}\right), \quad (3)$$

where $\bar{T}$ is the mean temperature, K is the thermal conductivity of the fluid, and C_p is the specific heat capacity.

To accurately represent the Reynolds stresses, an appropriate turbulence model is necessary. Since the flow in the computational domain includes rotation and flow separation, the SST k–ω turbulence model is selected. It is coupled with the Navier-Stokes equations for momentum and energy to provide reliable predictions of both flow characteristics and heat transfer behaviour (Li, Li, Tang, Fan, & Yang, 2023). In this approach, the Reynolds stress terms that arise from the RANS formulation are closed using the eddy-viscosity hypothesis, where the turbulent viscosity is obtained from the SST k–ω transport equations.

$$-\overline{u'_i u'_j} = v_t\left(\frac{\partial \bar{u}_i}{\partial x_j} + \frac{\partial \bar{u}_j}{\partial x_i}\right) - \frac{2}{3}k\delta_{ij} - \frac{2}{3}v_t\frac{\partial u_k}{\partial x_k}\delta_{ij} \quad (4)$$

The turbulent kinetic energy (k)

$$\nabla.(\rho\vec{u}k) = \nabla.\left[\left(\mu + \frac{\mu_t}{\sigma_k}\right)\nabla k\right] + G_k - Y_k. \quad (5)$$

The specific dissipation rate (ω)

$$\nabla.(\rho\vec{u}\omega) = \nabla.\left[\left(\mu + \frac{\mu_t}{\sigma_\omega}\right)\nabla\omega\right] + G_\omega - Y_\omega + D_\omega. \quad (6)$$

In these equations, G_k denotes the rate of turbulent kinetic energy generation resulting from the mean velocity gradients, whereas G_ω represents the production rate of ω associated with the mean flow. The terms Y_k and Y_ω account for the dissipation of k and ω due to turbulence effects. The turbulent viscosity μ_t is incorporated into the momentum and energy equations, influencing the Reynolds stresses and enhancing the effective thermal diffusion.

2.3. Boundary conditions

Inlet:

$$T = 298\ \text{K}, u = \frac{Re\mu}{\rho D_h}, Re = 10000 - 30000, I = 5\%.$$

Walls:

$$u{=}v{=}0,\ K_{cu} = 387.6\ \text{W/m K},$$

$$-K\frac{\partial T}{\partial y} = \begin{cases} 0, \text{smooth walls} \\ q_w = 10000\ \text{W/m}^2, \text{corrugated section} \end{cases}.$$

Outlet:

$$\frac{\partial u}{\partial x} = 0;\ \ \frac{\partial v}{\partial x} = 0;\ \ \frac{\partial T}{\partial x} = 0;\ P = P_{atm}.$$

2.4. Evaluation parameters

The pressure loss across the channel was determined using the following relation:

$$\Delta P = P_{in} - P_{out}. \tag{7}$$

The average Nusselt number (Nu) is obtained as follows (Abbasian Arani & Amani, 2013)

$$Nu = \frac{h\,D_h}{K}, \tag{8}$$

where h represents the convective heat transfer coefficient (W/(m²·K)), K is the thermal conductivity of the working fluid (W/(m K)), and D_h denotes the hydraulic diameter (m) of the corrugated passage, expressed as (Pehlivan, 2013).

$$D_h = H + h. \tag{9}$$

The friction factor (f) is calculated using the following equation (Heyhat, Kowsary, Rashidi, Momenpour, & Amrollahi, 2013):

$$f = \frac{2D_h\Delta P}{L\rho u^2}. \tag{10}$$

To quantify the increase in pressure loss caused by the VGs relative to that of a plain wavy channel, the pressure drop ratio (PR) is defined as (Mehta & Pati, 2020):

$$f = \frac{2D_h \Delta P}{L\rho u^2}, \tag{11}$$

where ΔP_{VGs} and ΔP_{WVGs} are the pressure drops in channels with and without VGs, respectively.
The percentage enhancement (PE) quantifies the improvement in heat transfer when VGs are applied and is given by (Mehta, Pati, & Baranyi, 2022):

$$PE = \frac{(Nu_{VGs} - Nu_{WVGs})}{Nu_{WVGs}} 100, \tag{12}$$

where Nu_{VGs} and Nu_{WVGs} denote the Nu for channels with and without VGs.
The overall thermal–hydraulic performance was assessed using the Performance Evaluation Criterion (PEC) (Akbarzadeh, Rashidi, & Esfahani, 2017):

$$PEC = \frac{\frac{Nu_{VGs}}{Nu_{WVGs}}}{\left(\frac{\Delta P_{VGs}}{\Delta P_{WVGs}}\right)^{\left(\frac{1}{3}\right)}}. \tag{13}$$

2.5. Numerical procedure

This study was carried out using ANSYS Fluent, a commercial CFD package based on the Finite Volume Method (FVM), which ensures conservation of mass, momentum, and energy in each control volume (Hasan & Hriczó, 2025). A Pressure-Based Coupled Solver (PBCS) [36] was used to solve the governing equations of continuity, momentum, and energy in a fully coupled manner. Convergence was achieved when the energy residuals fell below 10^{-6}, while the residuals for momentum, continuity, and turbulence equations were below 10^{-4}. Second-order upwind schemes were applied for improved numerical accuracy, and the least-squares cell-based method was used for gradient evaluation.

3. MESH INDEPENDENCE AND VALIDATION

The mesh plays a crucial role in determining the accuracy of the numerical results. A mesh independence test was conducted to identify the coarsest grid capable of producing reliable and accurate results. Five different mesh configurations were examined, with the total number of nodes varying between 98,037 and 557,168. To better capture the near-wall effects, ten inflation layers were generated adjacent to the channel walls (Figure 2) and around the VGs to capture the boundary layer

development and local velocity gradients with high precision in these regions. The relative error between successive meshes was calculated using (14) as described in (Shafiei, Hekmat, & Saharkhiz, 2022), where M_{i+1} denotes the current result and M_i represents the preceding Nu value

$$\text{Error}(\%) = \left|\frac{M_{i-}M_{i+1}}{M_{i+1}}\right| \cdot 100 \quad (14)$$

A notable reduction in error was observed in the final configuration, in which a mesh comprising 392,205 nodes (see Table 1) provided sufficient accuracy and was therefore adopted for the numerical analysis.

Table 1
Mesh independence

Mesh	Number of nodes	Nusselt number	Error (%)
1	98037	198.41	
2	148639	196.72	0.85
3	226732	195.46	0.64
4	392205	194.45	0.51
5	557168	193.46	0.50

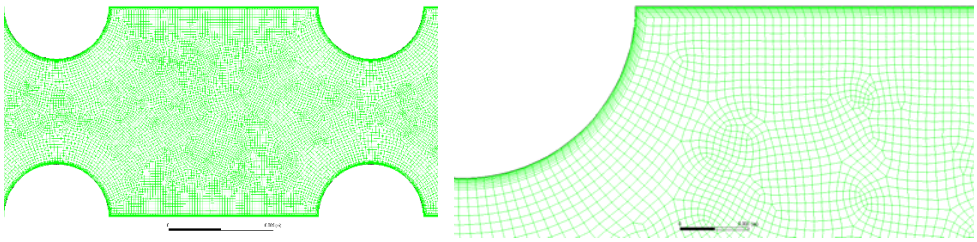

Figure 2. *Computational mesh*

To ensure the reliability of the simulation results, a validation study was conducted prior to the main analysis. The model was compared with the experimental work of (Ajeel R. , et al., 2019), who investigated a semi-circular corrugated channel under similar conditions. Figure 3 shows the variation in the average Nu over a Re range of 10,000 - 30,000, indicating that the numerical predictions are in good agreement with the experimental data. This close agreement validates the precision of the

numerical setup and the suitability of the selected modelling method for estimating heat transfer in corrugated channels. It is important to note that this validation was conducted for the baseline case (channel without VGs). An additional comparison with a numerical study incorporating VGs (Their, Hamad abed, Azeez, & Mohsin, 2023) further supported the robustness and accuracy of the proposed method. Moreover, the ΔP results obtained from the simulation were validated against experimental data (Ajeel, Salim, & Hasnan, 2019), with deviations remaining below 13%, demonstrating the reliability of the hydraulic performance prediction (Table 2).

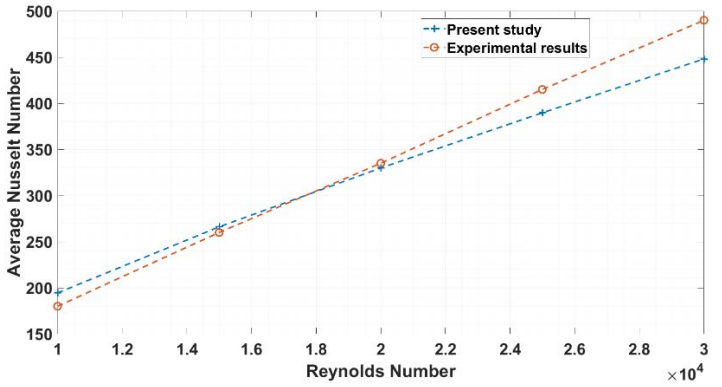

a)

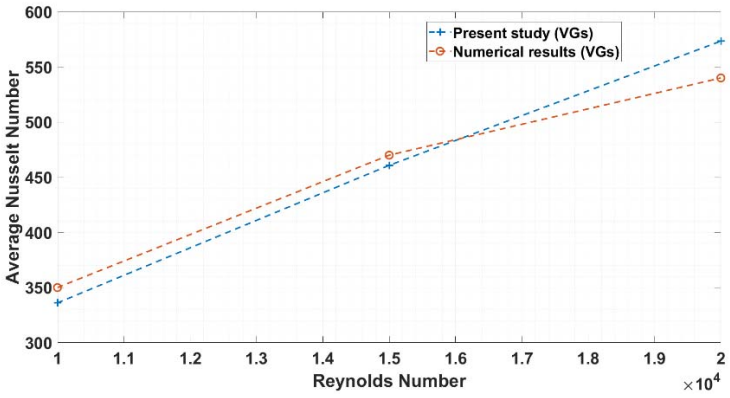

b)

Figure 3. *Validation of the present CFD results against literature data in terms of average Nusselt number for channels with (a)) and without (b))vortex generators*

Table 2

Validation of CFD pressure drop against experimental data for the baseline channel, showing percentage deviations

Re	Friction Factor f	ΔP Numerical (Pa)	ΔP Experimental (Pa)	Difference %
10000	0.0204	148	132	12.1%
20000	0.0153	450	400	12.5%
30000	0.0131	872	800	9.0%

4. RESULTS AND DISCUSSION

Figure 4 presents the isotherm contours and streamlines for the different VG positions. The position of the VGs plays a crucial role in the thermal-hydraulic performance of the channel. At d = –2. The position of the VGs eliminated much of the thermal boundary layer, especially near the corrugation corners. This was also evident in the streamlines, where the recirculation zone at the corner almost disappeared. This is mainly because the VG is located close to the corrugation entrance, where the flow is strongly redirected and the boundary layer is more easily disturbed. However, when the VGs was moved to the middle (d = 0) or further downstream (d = +2). The effect gradually weakened thereafter, and larger recirculation zones appeared at the corrugation corners. In these cases, the flow has already developed inside the corrugation, reducing the VG influence on the corner region. In these cases, the flow has already partially adapted to the corrugated geometry before reaching the VG, reducing its ability to disrupt the boundary layer and suppress the corner separation region. Placing the VGs at d = –2 also generated a larger recirculation zone in the centre of the channel. This enhanced fluid mixing and increased the turbulence. This improved the heat transfer on the other hand. This configuration significantly increased the pressure drop across the reactor. The stronger flow disturbance at this location increases friction losses, which explains the higher pressure penalty. Conversely, moving the VGs to d = +2 reduced the central recirculation, leading to a lower pressure penalty, less mixing, and weaker thermal performance.

Figu shows the x-velocity and turbulent kinetic energy (TKE) profiles along the vertical line at the middle of the corrugated section for various VG positions. When VGs is placed at d = 0. The velocity near the walls exhibited the greatest increase. Along the middle line of the channel, the velocity becomes negative owing to the influence of the central recirculation. In contrast at d = –2 the velocity along this line also decreased to a negative value.

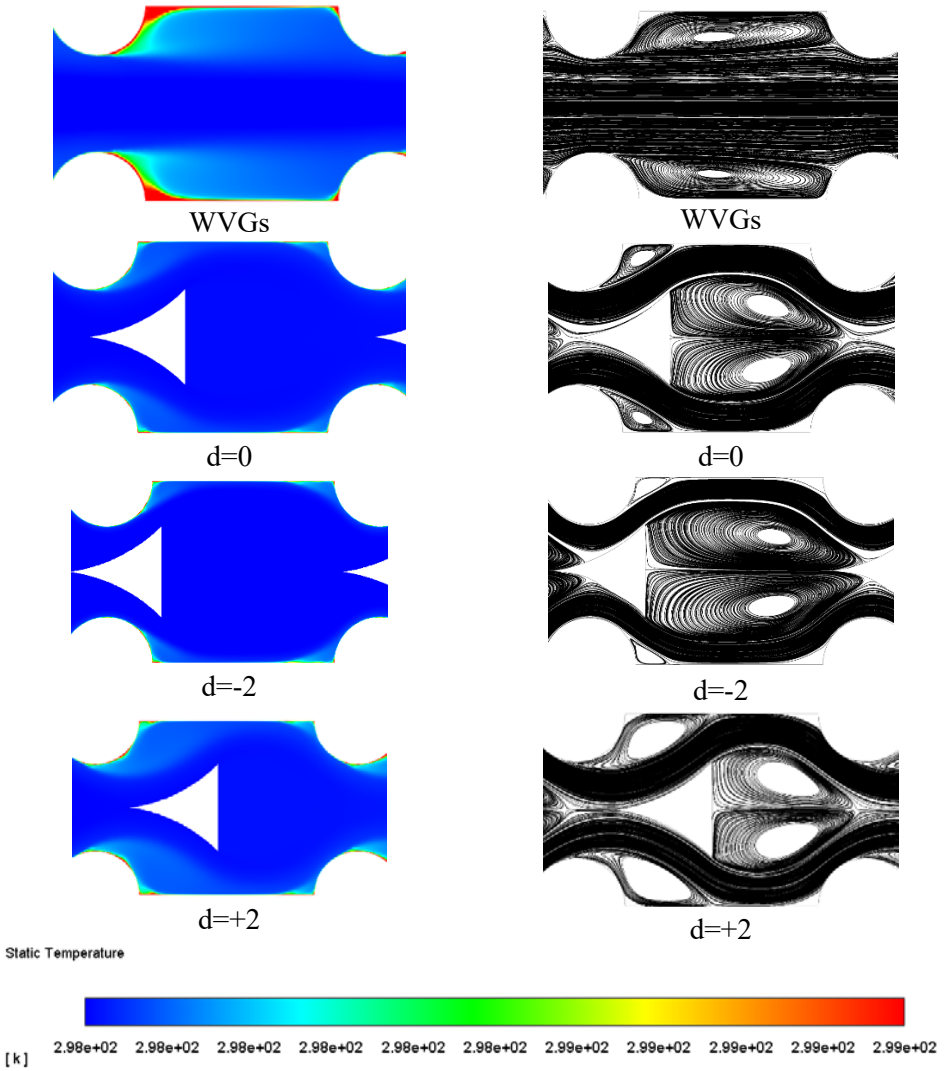

Figure 4. *Isotherm contours and streamlines illustrating the effect of different VG positions on flow and heat transfer*

However, the effect was stronger because of the larger recirculation zone formed upstream (Figure 4). This indicates that positioning the VG upstream strengthens the vortex development and promotes earlier flow reversal within the core region. For d = +2 recirculation was still observed. However, the line passes through the centre

of the recirculation zone. The velocity captured along that line was close to zero rather than negative values. This suggests that the recirculation becomes weaker and more confined when the VG is shifted downstream. The turbulent kinetic energy profiles further highlight this effect. Both d = –2 and d = 0 produced significantly higher turbulence than d = +2, where a weaker recirculation zone results in much lower turbulence. Along the middle line d = 0 exhibited the highest turbulence intensity. This is because the flow is forced to divide and concentrate more strongly around the VGs at this location. This resulted in a vigorous mixing. Higher turbulence levels increase momentum exchange between the core flow and near-wall region, which contributes directly to enhanced convective heat transfer.

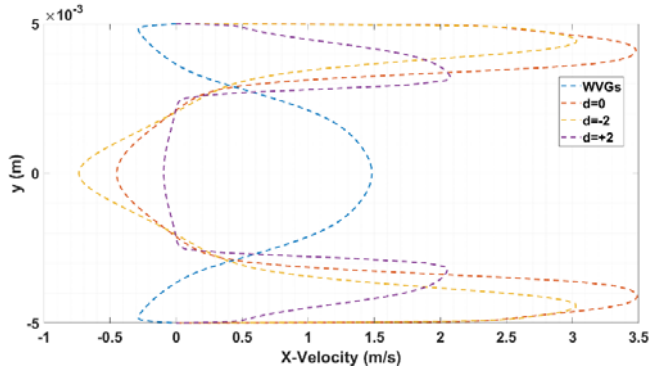

a)

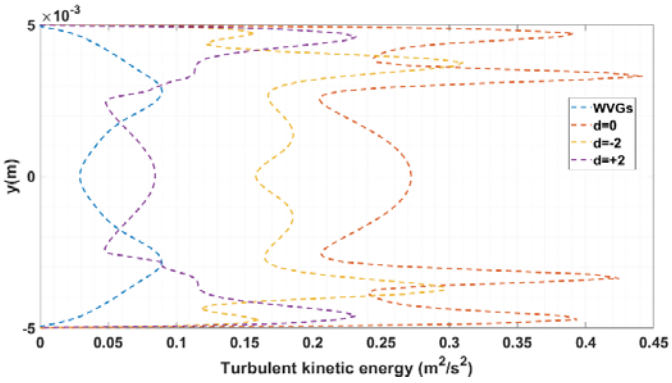

b)

Figure 5. *Profiles along the vertical line at the mid-length of the corrugated section: (a) x-velocity, (b) turbulent kinetic energy*

Figure shows the shear stress distribution along the bottom corrugated wall for different VG positions. For d = 0 the shear stress reached its peak value at the middle of the corrugated wall. In contrast at d = –2 the highest values were observed near the corners. This is consistent with the behaviour observed in the streamline and velocity profile. This indicates that placing the VG upstream enhances the near-wall flow acceleration at the corrugation entrance, which increases the local velocity gradient and therefore the shear stress near the corners. Each position has its own influence enhancing wall-fluid contact in different regions of corrugation. Case d = +2 exhibited the weakest overall shear stress, indicates a reduced interaction between the fluid and wall compared with the other cases. The lower shear stress in this case suggests weaker momentum transfer near the wall, which explains the lower heat transfer enhancement. The corresponding peak values are listed in Table 3.

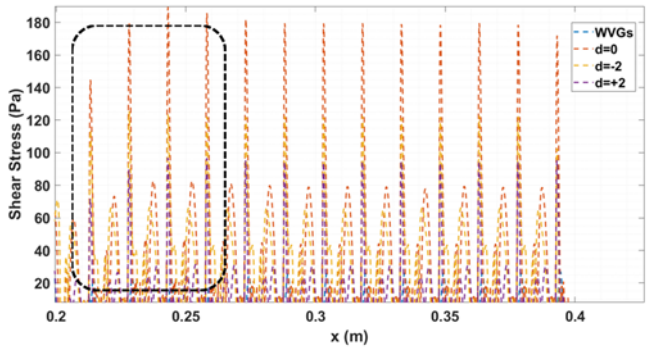

a)

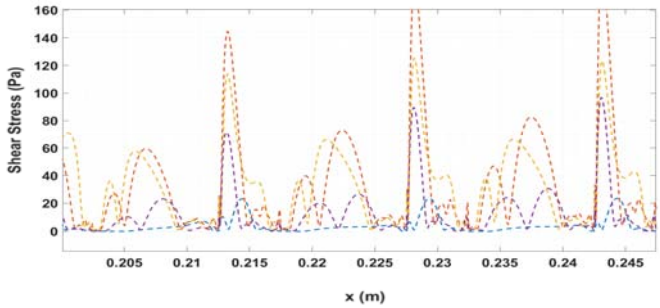

b)

Figure 6. *Distribution of wall shear stress along the corrugated section: a) full wall distribution, b) zoomed-in region*

Table 3

Peak wall shear stress along corrugated wall

Case	Peak shear stress (Pa)	Average trend (approx.)
WVGS	~40-50	Low; peaks mainly at pitch
d = –2	~150-160	High at corners; strong wall contact
d = 0	~170-180	Highest in middle; strong uniformity
d = +2	~120-130	Moderate; weaker overall effect

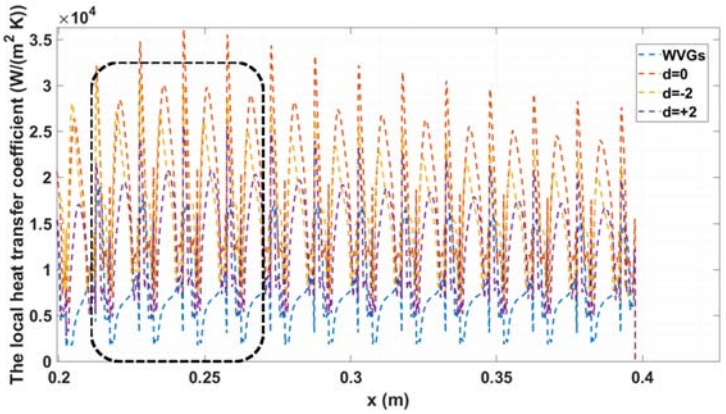

a)

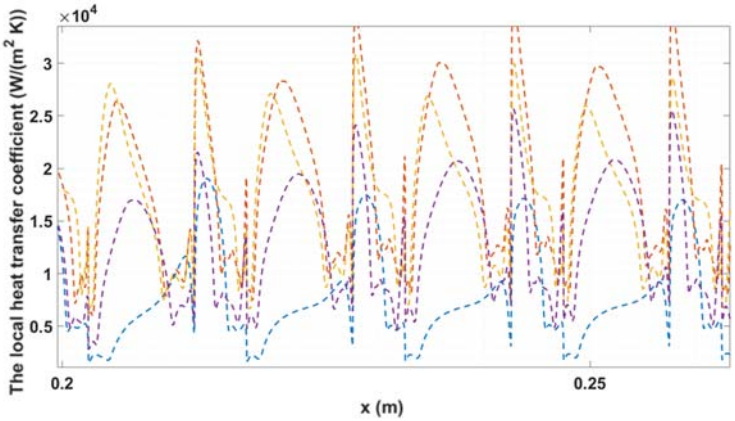

b)

Figure 7. *Distribution of local heat transfer coefficient along the corrugated section: a) full wall distribution, b) zoomed-in region*

Figure 7 shows the local h along the bottom wall of the corrugated section for different VG positions. At d = –2 the VGs significantly increased the h at the corrugation corners compared with other cases. This is mainly because the upstream placement strengthens the flow impingement and mixing near the corrugation entrance, which intensifies the thermal boundary layer disruption in these regions. In contrast at d = 0 the enhancement was higher in the middle of the corrugated wall but was less pronounced at the corners. The case with d = +2 shows the weakest overall performance due to low turbulence and reduced velocity near the wall. This prevents the fluid from being effectively driven into these areas. As a result, the thermal boundary layer remains thicker, leading to lower local heat transfer levels. The peak values for each configuration are listed in Table 4.

Table 4

Peak local heat transfer coefficient along corrugated wall

Case	**Peak local h (×10⁴ W/m²K)**	**Average trend (approx.)**
WVGS	~0.9-1.0	Peaks only at pitch; weak elsewhere
d = –2	~3.2-3.4	Strong at corners; enhanced spread along wall
d = 0	~3.6	Higher in middle; weaker at corners
d = +2	~2.3-2.4	Moderate; weaker overall due to low turbulence

Table 5

Overview of average Nu and pressure drop for various VG positions across different Re

	Nu				**Δ*P***			
Re	WVGs	d = 0	d = –2	d = +2	WVGs	d = 0	d = –2	d = +2
10000	194.45	336.1	399.09	323.59	1123.93	8191.48	14394.38	7966.91
15000	266.09	460.78	555.01	460.43	2503.78	17921.05	31703.37	17928.72
20000	329.86	573.39	700.26	572.15	4336.47	30374.9	54411.41	30392.25
25000	389.69	680.64	845.48	680.06	6637.79	45502.82	82593.7	45527.93
30000	448.08	791.71	993.64	789.9	9457.5	63726.09	117250.8	63767.62

Figure 8 shows the variation in the average Nu and ΔP with the Re for different VG positions. The results indicate a clear difference in the heat transfer when the VGs is inserted. The case with d = –2 achieved the highest average Nu was significantly higher than that of the other positions. This improvement is linked to the stronger enhancement at the corrugation corners. This is reflected in the overall average performance. This confirms that positioning the VG upstream provides a longer effective region for mixing and boundary layer disruption along the corrugated

section. The cases with d = 0 and d = +2 show similar results, with d = +2 slightly lower and d = 0 slightly higher. However, the differences are relatively small compared to the gap with d = –2. For ΔP the position at d = –2 again shows the highest penalty for the same reason as above. As the VGs near the entrance created a large recirculation zone that strongly resisted flow. The early flow diversion increases flow blockage and friction losses, leading to a larger pressure drop. In contrast d = 0 and d = +2 resulted in lower pressure drops with d = +2 being slightly higher than that for d = 0. This is because placing the VGs closer to the next corrugation entrance restricts the flow. The corresponding values are listed in Table 5.

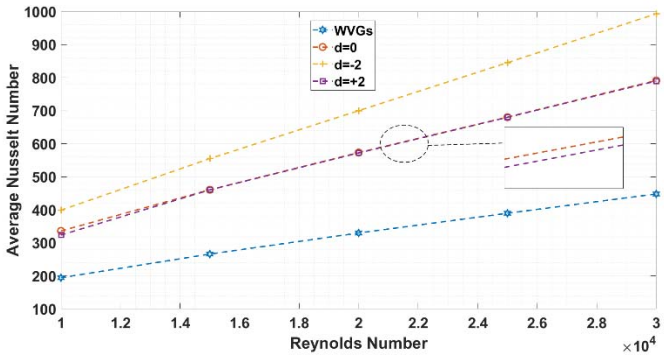

a)

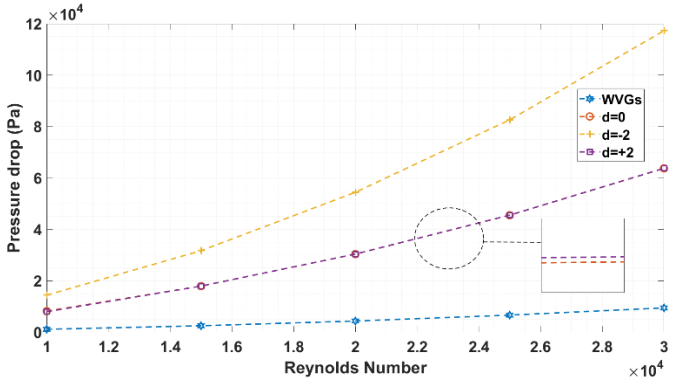

b)

Figure 8. *Variation of (a) average Nusselt number and (b) pressure drop with Reynolds number for different VG positions*

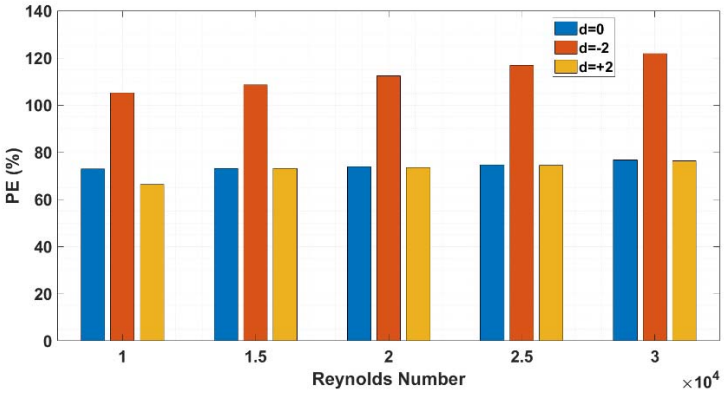

a)

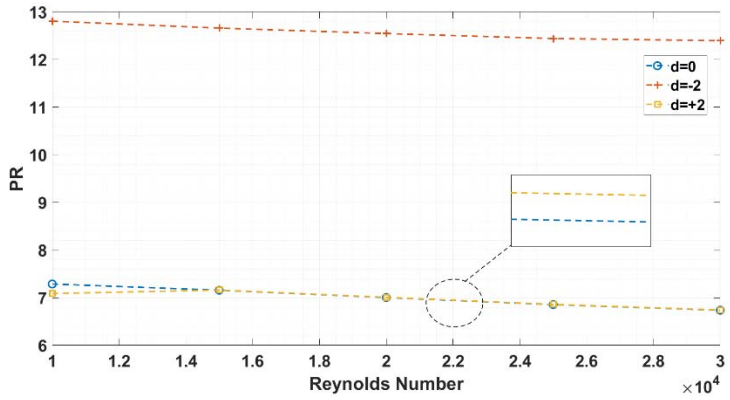

b)

Figure 9. *Variation of (a) Performance Enhancement and (b) Pressure Ratio with Reynolds number for different VG positions*

Figure 9 presents the PE and PR as functions of the Re for different VG positions. The heat transfer enhancement reached approximately 121 % for d = –2 compared to 77 % and 76 % for d = 0 and d = +2, respectively. The enhancement was more pronounced at higher Re than at lower ones highlighting that the use of VGs is especially effective in higher-flow regimes. At higher Re, the increased inertial forces strengthen vortex formation and mixing, which improves the heat transfer

enhancement. On the other hand, the PR exhibited the highest penalty at d = –2 reaching nearly 12.5 times the baseline. This was significantly higher than that of the other positions which is approximately seven times. This confirms that the upstream placement produces the strongest flow disturbance and recirculation, resulting in higher friction and pressure losses. As the Re increased, the difference in the PR between the cases decreased. This indicates that at higher Re, the relative impact of VGs on pressure loss is reduced compared with the lower Re. This behaviour can be attributed to the dominance of the main flow momentum at high Re, which reduces the relative contribution of the VG-induced losses.

Table 6

PEC for different VG positions at various Re

	PEC		
Re	d=0	d=-2	d=+2
10000	0.89	0.87	0.86
15000	0.89	0.89	0.89
20000	0.90	0.91	0.90
25000	0.91	0.93	0.91
30000	0.93	0.96	0.93

Figure presents the PEC as a function of the Re for different VG positions. The configuration with d = 0 showed higher PEC values only in the Re range of 10000 - 15000. In contrast, the d = –2 configuration achieves higher PEC values overall, particularly at Re = 30000, where it reaches 0.96, which is very close to the ideal value of 1, indicating an excellent balance between heat transfer enhancement and pressure drop. This configuration also exhibited favourable PE results, suggesting that a VG with spacing S = 5 mm represents an optimal position and size. Such a VG can be implemented in real-world applications, such as heat exchangers, to significantly improve thermal performance while maintaining acceptable pressure losses. Similar trends were reported by (Asaadi & Abdi, 2021), who studied vortex generators in a rectangular channel and obtained PEC values in the range of 0.85 - 0.94. In the present study, the PEC values (up to 0.96) are very close to unity, indicating a near-optimal thermal-hydraulic balance. Although PEC is slightly below 1, this is still considered highly favourable in heat transfer enhancement studies, as it reflects a significant heat transfer improvement (up to 121%) achieved with a manageable increase in pressure drop. Therefore, values slightly below unity are acceptable and even desirable when strong thermal enhancement is prioritized over moderate hydraulic penalties. The key results are presented in Table 6.

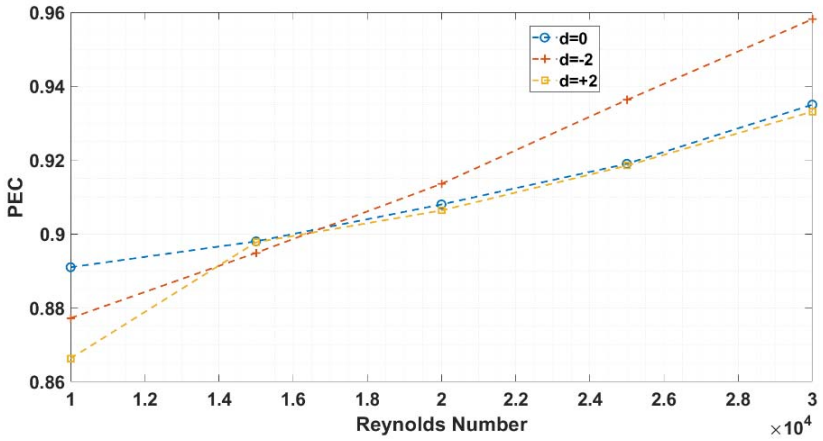

Figure 10. *Variation of Performance Evaluation Criterion with Reynolds number for different VG positions*

5. CONCLUSIONS

This study investigated the influence of VG position on the flow and heat transfer performance in a corrugated channel. The analysis included isotherms, streamlines, velocity fields, turbulent kinetic energy, wall shear stress, local heat transfer coefficient, and average Nusselt number.

The results show that adding VGs significantly improves heat transfer by disrupting the thermal boundary layer and enhancing fluid mixing compared with the plain corrugated channel. The position of the VGs has a strong effect on performance. When placed near the corrugation entrance (d = –2), the system achieved the highest heat transfer enhancement of about 121 % and a maximum PEC of 0.96. This improvement is due to stronger mixing and reduced recirculation zones. However, this case also caused the highest pressure-drop, about 12.5 times the baseline. The positions d = 0 and d = +2 gave lower heat transfer enhancement (around 77% and 76%) but with reduced pressure losses.

The study is based on a two-dimensional numerical model using water as the working fluid and considers a single corrugation geometry with limited VG positions. Three-dimensional effects and other working fluids were not included, which may slightly limit the general applicability of the results.

REFERENCES

Abbasian Arani, A., & Amani, J. (2013). Experimental investigation of diameter effect on heat transfer performance. *Experimental Thermal and Fluid Science, 44*, 520-533. https://doi.org/10.1016/j.expthermflusci.2012.08.014

Ajeel, R., Salim, W.-I., & Hasnan, K. (2019). Thermal performance comparison of various corrugated channels using. *Alexandria Engineering Journal, 58*(1), 75-87. https://doi.org/10.1016/j.aej.2018.12.009

Ajeel, R., Salim, W.-I., Sopian, K., Yusoff, M., Hasnan, K., Ibrahim, A., & Al-Waeli, A. (2019). Turbulent convective heat transfer of silica oxide nanofluid through. *International Journal of Heat and Mass Transfer, 145*(118806), 118806. https://doi.org/10.1016/j.ijheatmasstransfer.2019.118806

Akbarzadeh, M., Rashidi, S., & Esfahani, J. (2017). Influences of corrugation profiles on entropy generation, heat transfer,. *Applied Thermal Engineering, 116*, 278-291. https://doi.org/10.1016/j.applthermaleng.2017.01.076

Akcay, S. (2022). Numerical analysis of heat transfer improvement for pulsating flow in a. *International Communications in Heat and Mass Transfer, 134*(105991), 105991. https://doi.org/10.1016/j.icheatmasstransfer.2022.105991

Asaadi, S., & Abdi, H. (2021). Numerical investigation of laminar flow and heat transfer in a channel. *Journal of Thermal Analysis and Calorimetry, 145*(5), 2795-2808. https://doi.org/10.1007/s10973-020-09795-5

Brodnianská, Z., & Kotšmíd, S. (2023). Heat transfer enhancement in the novel wavy shaped heat exchanger channel. *Applied Thermal Engineering, 220*(119720), 119720. https://doi.org/10.1016/j.applthermaleng.2022.119720

Elshafei, E., Awad, M., El-Negiry, E., & Ali, A. (2010). Heat transfer and pressure drop in corrugated channels. *Energy (Oxford, England), 35*(1), 101-110. https://doi.org/10.1016/j.energy.2009.08.031

Hasan, M., & Hriczó, K. (2025). Evaluation of a dual-purpose solar collector using mono-nanofluids: A CFD. *Pollack periodica*. https://doi.org/10.1556/606.2025.01394

Heyhat, M., Kowsary, F., Rashidi, A., Momenpour, M., & Amrollahi, A. (2013). Experimental investigation of laminar convective heat transfer and. *Experimental Thermal and Fluid Science, 44*, 483-489. https://doi.org/10.1016/j.expthermflusci.2012.08.009

Ismail, M., Ali, A., & Pereira, S.-C. (2025). Vortex generators in heat sinks: Design, optimisation, applications and. *Results in Engineering, 25*(104216), 104216. https://doi.org/10.1016/j.rineng.2025.104216

Kim, A. S. (2019). *Advanced Computational Fluid Dynamics for Emerging Engineering Processes - Eulerian vs. Lagrangian.* InTech.

Kotšmíd, S., & Brodnianská, Z. (2022). The effect of diameter and position of transverse cylindrical vortex. *Mathematics, 10*(23), 4546. https://doi.org/10.3390/math10234546

Li, X., Li, G., Tang, G., Fan, Y., & Yang, D. (2023). A generalized thermal deviation factor to evaluate the comprehensive. *Energy (Oxford, England), 263*(125710), 125710. https://doi.org/10.1016/j.energy.2022.125710

Mehta, S., & Pati, S. (2020). Numerical study of thermo-hydraulic characteristics for forced convective. *Journal of Thermal Analysis and Calorimetry, 141*(6), 2429-2451. https://doi.org/10.1007/s10973-020-09412-5

Mehta, S., Pati, S., & Baranyi, L. (2022). Effect of amplitude of walls on thermal and hydrodynamic characteristics. *Case Studies in Thermal Engineering, 31*(101796), 101796. https://doi.org/10.1016/j.csite.2022.101796

Modi, A., & Rathod, M. (2019). Comparative study of heat transfer enhancement and pressure drop for. *International Journal of Heat and Mass Transfer, 141*, 310-326. https://doi.org/10.1016/j.ijheatmasstransfer.2019.06.088

Naphon, P. (2007). Heat transfer characteristics and pressure drop in channel with V. *Energy Conversion and Management, 48*(5), 1516-1524. https://doi.org/10.1016/j.enconman.2006.11.020

Neves, F., Soares, A., & Rouboa, A. (2022). Forced convection heat transfer of nanofluids in turbulent flow in a flat. *Energy Reports, 8*, 1185-1195. https://doi.org/10.1016/j.egyr.2022.07.087

Omle, I., Askar, A., & Kovács, E. (2024). Impact of wall roughness elements type and height on heat transfer inside. *Pollack periodica, 19*(2), 146-153. https://doi.org/10.1556/606.2024.00986

Omle, I., Askar, A., & Kovács, E. (2024). Optimizing the design of container house walls using argon and recycled. *Buildings, 14*(12), 3944. https://doi.org/10.3390/buildings14123944

Omle, I., Kovács, E., & Bolló, B. (2023). The effect of surface triangular roughness inspired by nature with. *Heat Transfer Research*. https://doi.org/10.1615/heattransres.2023048854

Pehlivan, H. (2013). Experimental investigation of convection heat transfer in. *International Journal of Heat and Mass Transfer, 66*, 128-138. https://doi.org/10.1016/j.ijheatmasstransfer.2013.06.033

Pehlivan, H., Taymaz, I., & İslamoğlu, Y. (2013). Experimental study of forced convective heat transfer in a different. *International Communications in Heat and Mass Transfer, 46*, 106-111. https://doi.org/10.1016/j.icheatmasstransfer.2013.05.016

Promvonge, P., Promthaisong, P., & Skullong, S. (2022). Thermal performance augmentation in round tube with louvered V-winglet. *International Journal of Heat and Mass Transfer, 182*(121913), 121913. https://doi.org/10.1016/j.ijheatmasstransfer.2021.121913

Samadifar, M., & Toghraie, D. (2018). Numerical simulation of heat transfer enhancement in a plate-fin heat. *Applied Thermal Engineering, 133*, 671-681. https://doi.org/10.1016/j.applthermaleng.2018.01.062

Shafiei, H., Hekmat, M., & Saharkhiz, S. (2022). Comprehensive study of heat transfer enhancement in turbulent nanofluid. *Journal of the Brazilian Society of Mechanical Sciences and Engineering, 44*(12). https://doi.org/10.1007/s40430-022-03901-4

Shah, M., Pan, K., Ibrahim, M., Saeed, T., & Ibrahim, S. (2022). Numerical study and optimization of important parameters of non-Newtonian. *Engineering Analysis With Boundary Elements, 139*, 94-108. https://doi.org/10.1016/j.enganabound.2022.03.022

Shlash, B., & Koç, I. (2022). Turbulent fluid flow and heat transfer enhancement using novel vortex. *Advanced Research in Fluid Mechanics and Thermal Sciences, 96*(1), 36-52. https://doi.org/10.37934/arfmts.96.1.3652

Tanougast, A., & Hriczó, K. (2025, 9). Effect of Winglet-Designed Vortex Generators on Heat Transfer Performance in Corrugated Channels. *Applied Scientific Research, 5*(2), 5-14. https://doi.org/10.56131/tmt.2025.5.2.382

Tanougast, A., & Hriczó, K. (2025). Enhanced heat transfer in wavy channels with vortex generators: A CFD. *International Journal of Thermofluids, 30*(101405), 101405. https://doi.org/10.1016/j.ijft.2025.101405

Tanougast, A., & Hriczó, K. (2025). Numerical modeling of unsteady heat convection in turbulent flow. 180006. https://doi.org/10.1063/5.0286594

Tanougast, A., Bessaih, R., & Hriczó, K. (2025). Comparative study of different vortex generator designs in corrugated. *Results in Physics, 77*(108450), 108450. https://doi.org/10.1016/j.rinp.2025.108450

Tanougast, A., Omle, I., & Hriczó, K. (2025). Turbulent hybrid nanofluid flow in corrugated channels with vortex. *Fluids, 10*(10), 249. Retrieved from https://doi.org/10.3390/fluids10100249

Their, K., Hamad abed, T., Azeez, K., & Mohsin, M. (2023). Thermohydraulic performance study of the effect of winglet inserts and a. *Case Studies in Thermal Engineering, 52*(103707), 103707. https://doi.org/10.1016/j.csite.2023.103707

Wang, C.-C., & Chen, C.-K. (2002). Forced convection in a wavy-wall channel. *International Journal of Heat and Mass Transfer, 45*(12), 2587-2595. https://doi.org/10.1016/s0017-9310(01)00335-0

Wu, J., Liu, P., Yu, M., Liu, Z., & Liu, W. (2022). Thermo-hydraulic performance and exergy analysis of a fin-and-tube heat. *Revue generale de thermique [International Journal of Thermal Sciences], 172*(107274), 107274. https://doi.org/10.1016/j.ijthermalsci.2021.107274